Second-order recoupling of chemical-shielding and dipolar-coupling tensors under spin decoupling in solid-state NMR

Matthias Ernst,[a] Seth Bush, Andrew C. Kolbert,[b] and Alexander Pines
Materials Sciences Division, E. O. Lawrence Berkeley National Laboratory, 1 Cyclotron Road, Berkeley, California 94720 and Department of Chemistry, University of California, Berkeley, California 94720

(Received 18 March 1996; accepted 14 May 1996)

The source of the residual line broadening in continuous-wave (cw) decoupled spectra under magic-angle sample spinning conditions is reexamined. It is shown that an important contribution to the line broadening comes from a second-order recoupling of the heteronuclear dipolar-coupling tensor and the chemical-shielding tensor of the irradiated spin. Such an interference between the two tensors leads to a sum of a zeroth-rank, a second-rank, and a fourth-rank tensor component in the Hamiltonian. The zeroth-rank and the fourth-rank tensor components are not averaged out under magic-angle sample spinning (MAS) conditions, requiring the use of higher-order averaging such as double rotation (DOR) for obtaining narrow lines. This broadening is distinctly different from off-resonance decoupling effects which transform as a second-rank tensor and can be averaged out by MAS. The properties of this second-order recoupling as a source of structural information are explored, and the conditions for removing the broadening in systems with weak homonuclear dipolar-coupling networks are discussed. © *1996 American Institute of Physics.* [S0021-9606(96)01132-4]

I. INTRODUCTION

High-power continuous-wave (cw) irradiation remains the most common way to achieve heteronuclear spin decoupling[1–3] in solid-state nuclear magnetic resonance spectroscopy (NMR). It is generally accepted that for efficient decoupling the field strength must be greater than the magnitude of both the heteronuclear *and* the homonuclear dipolar interactions. In solids with strongly coupled homonuclear spin systems the flip–flop fluctuations of the homonuclear spins lead to an additional modulation of the heteronuclear dipolar coupling which results in a further narrowing of the observed line.[2] It has been shown that by applying the decoupling field off-resonance such that the effective field is inclined at an angle of 54.74° (magic angle) to the static magnetic field, the homonuclear interactions are quenched. The reduced or vanishing homonuclear dipolar interactions lead to a broadening of the decoupled heteronuclear line.[2] In recent years there has been renewed interest in the understanding of cw decoupling[4–6] and in developing improved decoupling schemes[7] that decrease the residual linewidth in decoupled spectra under magic-angle sample spinning (MAS).[8–10] A detailed discussion of the various contributions to the line width of solid-state NMR spectra under high-power cw decoupling and MAS has been reported in the literature.[11]

In this paper we seek to clarify the source of the broadening observed in systems with weak homonuclear dipolar-coupling networks. As a model system we investigate an isolated two-spin system where cw decoupling does not lead to a sharp line but gives rise to a splitting and a broadening of the line (Fig. 1). This effect can be explained as a second-order recoupling of the heteronuclear dipolar-coupling tensor and the chemical-shielding tensor of the irradiated spin in the rotating frame. This second-order effect cannot be averaged out by MAS since the coupling of the two tensors leads to a sum of a zeroth-rank, a second-rank, and a fourth-rank tensor. However, by using advanced spatial averaging techniques like dynamic-angle spinning (DAS) or double rotation (DOR)[12–14] it is possible to average out both the second-rank and the fourth-rank contributions to the Hamiltonian simultaneously leaving only the isotropic (zeroth-rank tensor) part. These crossterms are mentioned in passing in Ref. 7 but they are not elaborated on and there is no discussion of the effects they cause.

An effect related to the second-order recoupling for the case of isotropic interactions is well known in liquid-state NMR as ''off-resonance decoupling.''[15,16] There one obtains a scaled isotropic J coupling when the irradiation of the cw-decoupling field is off-resonance. However, in our case new and interesting features appear because the interference is between two second-rank tensors and not two scalar quantities. The recoupling we describe in this paper is also different from off-resonance decoupling effects in solids. Off-resonance irradiation in solids results in the coupling of a scalar quantity (resonance offset) and a second-rank tensor (dipolar coupling) leading to a recoupling which is fully described by a second-rank tensor. Therefore, such a contribution to the line broadening is averaged out under MAS conditions and will not lead to an observable broadening of the line.

Second-order effects in the laboratory frame due to the truncation of the Hamiltonian by the Zeeman field are well

[a]Present address: Laboratory for Physical Chemistry, University of Nijmegen, Toernooiveld, NL-6525 ED Nijmegen, The Netherlands.
[b]Present address: DSM Copolymer Inc., P.O. Box 2591, Baton Rouge, LA 70821.

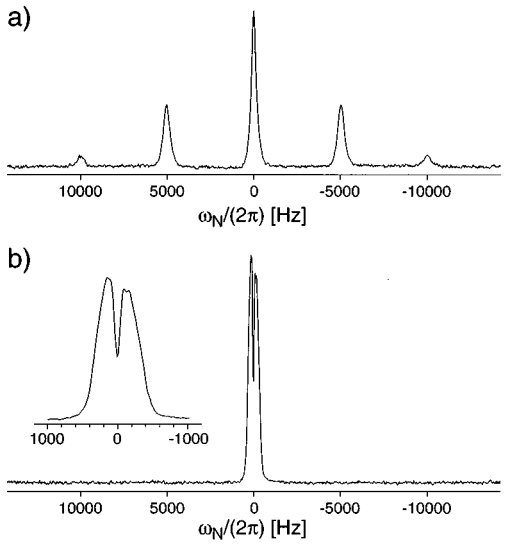

FIG. 1. ^{15}N spectra of fully ^{15}N-labeled tri-(trideuteromethyl)-ammoniumchloride without (a) and with (b) cw decoupling of the protons during acquisition. The sample was spinning at the magic angle with $\omega_r/(2\pi)=5$ kHz and the rf field strength was $\omega_{rf}/(2\pi)=71.5$ kHz. Without proton irradiation (a) the spectrum shows a single sharp line with spinning sidebands. Under proton cw decoupling (b) the line is split and broadened due to the second-order recoupling of the chemical-shielding tensor of the irradiated spin and the heteronuclear dipolar-coupling tensor. The two spectra clearly illustrate that cw decoupling does not give the desired result in isolated heteronuclear two-spin systems.

known in solid state NMR.[1,2,17] The best known example is the second-order quadrupolar shift[18] but other examples such as a shift originating from the dipolar coupling have been observed experimentally.[19,20] Recently we have described an isotropic second-order dipolar shift in the rotating frame[21] which can be substantially larger than the second-order dipolar shifts in the laboratory frame because the interaction is scaled by the rf field and not by the Zeeman field. The second-order dipolar shift in the rotating frame is very closely related to the second-order recoupling of the dipolar coupling and the chemical-shielding tensors. However, since the Hamiltonian describing the second-order dipolar shift commutes with the *S*-spin subspace of the Hamiltonian, it has no influence on the spectrum of the observed spin.

Some years ago another related effect called ''rotary resonance recoupling'' (R^3)[22–25] was described which also leads to the recoupling of the dipolar-coupling and the chemical-shielding tensors. The condition for recoupling in the R^3 experiment is that the rf field is a small integer multiple of the spinning speed and results in a broadening of the usually sharp sideband spectrum. The broadening was explained as an interference between the decoupling field and the mechanical sample rotation. In our experiment, however, the decoupling field strength is typically 1 order of magnitude larger than the spinning speed which results in a separation of the time scales of the two averaging processes. These two averaging processes will be treated as independent in the theoretical treatment in this publication.

The second-order recoupling of the dipolar-coupling and the chemical-shielding tensors has two aspects. First, it contains valuable information about the orientation of the two tensors in isolated two-spin systems. This information can be extracted by fitting the second-order spectrum with the analytical solution of the expected line shape. Second, if high resolution is required in a dimension of a multidimensional experiment, it is necessary to remove the second-order recoupling. This can be achieved by using decoupling sequences which are symmetric in the average-Hamiltonian sense[1] as will be shown in Sec. II. It could be argued that systems with weak homonuclear dipolar-coupling networks are not very common and as such not important. With increasing MAS spinning speeds, however, more and more substances will fall into the category of weak homonuclear dipolar-coupling networks. In addition, the increased use of double isotopic labeling to obtain structural information by solid-state NMR techniques, creates another category of substances with weak homonuclear dipolar-coupling networks.

The material in this paper is presented as follows. Section II describes the theoretical treatment of the observed effects and analyzes its features under static, MAS and DAS conditions. In Sec. III we present experimental results for a model two-spin system. Numerical simulations to illustrate some additional aspects of the second-order recoupling effect are shown in Sec. IV.

II. THEORY

We start our theoretical discussion of the second-order recoupling from the truncated high-field rotating-frame Hamiltonian for an isolated two-spin system under continuous-wave (cw) rf irradiation of the I spin[2]

$$\mathscr{H}=\omega_D(\Omega_D)\cdot 2S_zI_z+\omega_S(\Omega_S)\cdot S_z+\omega_I(\Omega_I)\cdot I_z+\omega_{\rm rf}\cdot I_x\,. \tag{1}$$

The Hamiltonian includes the heteronuclear dipolar-coupling tensor, the chemical-shielding tensors for both the S and the I spin, and the rf term. The orientation-dependent dipolar-coupling tensor is defined in the rotating frame as

$$\omega_D(\Omega_D)=-\frac{\mu_0}{4\pi}\cdot\frac{\gamma_S\gamma_I\hbar}{r_{SI}^3}\cdot\frac{3\cos^2\beta_D-1}{2}$$

$$=\frac{\delta_D}{2}\cdot P_2(\cos\beta_D), \tag{2}$$

where δ_D is the anisotropy of the dipolar-coupling tensor. The set of three Euler angles $\Omega_D=(\alpha_D,\beta_D,\gamma_D)$ describes the orientation of the dipolar-coupling tensor in the laboratory frame. The chemical-shielding tensor of the I spin is defined as

$$\omega_I(\Omega_I)=\delta_I\cdot\left[\frac{3\cos^2\beta_I-1}{2}+\frac{\eta_I}{2}\cdot\sin^2\beta_I\cdot\cos(2\alpha_I)\right]$$

$$+\omega_I^{\rm iso}, \tag{3}$$

where δ_I is the anisotropy and η_I is the asymmetry of the tensor. $\omega_I^{\rm iso}$ is the isotropic resonance offset and $\Omega_I=(\alpha_I,\beta_I,\gamma_I)$ is the set of three Euler angles describing the orientation of the chemical-shielding tensor in the labo-

ratory frame. An analogous expression can be written down for the S spin by replacing all I-spin indices with S. We can analytically diagonalize the Hamiltonian of Eq. (1) and obtain the following time-domain signal for an initial density operator $\sigma(0)=S_x$ and a phase-sensitive detection operator S^-:

$$\mathcal{S}(\Omega_D,\Omega_I,\Omega_S,t)=\sum_{m=1}^{4}\mathcal{S}_m(\Omega_D,\Omega_I,\Omega_S)\cdot e^{+i\cdot\omega_m(\Omega_D,\Omega_I,\Omega_S)\cdot t}. \tag{4}$$

The four transition frequencies are symmetric around $\omega_S(\Omega_S)$ and are given by[26]

$$\omega_{1,2}(\Omega_D,\Omega_I,\Omega_S)=\omega_S(\Omega_S)\pm\frac{\omega_{\rm rf}}{2}\cdot\left[\sqrt{1+\left(\frac{\omega_D(\Omega_D)+\omega_I(\Omega_I)}{\omega_{\rm rf}}\right)^2}+\sqrt{1+\left(\frac{\omega_D(\Omega_D)-\omega_I(\Omega_I)}{\omega_{\rm rf}}\right)^2}\right] \tag{5}$$

and

$$\omega_{3,4}(\Omega_D,\Omega_I,\Omega_S)=\omega_S(\Omega_S)\pm\frac{\omega_{\rm rf}}{2}\cdot\left[\sqrt{1+\left(\frac{\omega_D(\Omega_D)+\omega_I(\Omega_I)}{\omega_{\rm rf}}\right)^2}-\sqrt{1+\left(\frac{\omega_D(\Omega_D)-\omega_I(\Omega_I)}{\omega_{\rm rf}}\right)^2}\right]. \tag{6}$$

The corresponding signal intensities of these four lines are

$$\mathcal{S}_{1,2}(\Omega_D,\Omega_I,\Omega_S)=\frac{1}{4}-\frac{1}{4}\left(1+\frac{4\omega_D(\Omega_D)^2\omega_{\rm rf}^2}{(\omega_D(\Omega_D)^2+\omega_I(\Omega_I)^2+\omega_{\rm rf}^2)^2}\right)^{-1/2} \tag{7}$$

and

$$\mathcal{S}_{3,4}(\Omega_D,\Omega_I,\Omega_S)=\frac{1}{4}+\frac{1}{4}\left(1+\frac{4\omega_D(\Omega_D)^2\omega_{\rm rf}^2}{(\omega_D(\Omega_D)^2+\omega_I(\Omega_I)^2+\omega_{\rm rf}^2)^2}\right)^{-1/2}. \tag{8}$$

In the limit of strong decoupling the intensities $\mathcal{S}_1(\Omega_D,\Omega_I,\Omega_S)$ and $\mathcal{S}_2(\Omega_D,\Omega_I,\Omega_S)$ are small, and the transition frequencies $\omega_1(\Omega_D,\Omega_I,\Omega_S)$ and $\omega_2(\Omega_D,\Omega_I,\Omega_S)$ will therefore be neglected in the further discussion. The intensities $\mathcal{S}_3(\Omega_D,\Omega_I,\Omega_S)$ and $\mathcal{S}_4(\Omega_D,\Omega_I,\Omega_S)$ tend towards 0.5 for strong decoupling fields. To analyze the coupling of the two tensors in Eq. (6), we expand the square root as a power series. Assuming that the decoupling field strength is much larger than the dipolar-coupling or the chemical-shielding tensors we obtain

$$\omega_{3,4}(\Omega_D,\Omega_I,\Omega_S)=\omega_S(\Omega_S)\pm\frac{\omega_{\rm rf}}{2}\cdot\left[1+\frac{1}{2}\cdot\left(\frac{\omega_D(\Omega_D)+\omega_I(\Omega_I)}{\omega_{\rm rf}}\right)^2+\cdots-1-\frac{1}{2}\cdot\left(\frac{\omega_D(\Omega_D)-\omega_I(\Omega_I)}{\omega_{\rm rf}}\right)^2-\cdots\right]. \tag{9}$$

Truncating Eq. (9) after the first two terms is equivalent to second-order perturbation theory and leads to the following approximate expression for the transition frequencies:

$$\omega_{3,4}(\Omega_D,\Omega_I,\Omega_S)\approx\omega_S(\Omega_S)\pm\left(\frac{\omega_D(\Omega_D)\omega_I(\Omega_I)}{\omega_{\rm rf}}\right). \tag{10}$$

Equation (10) describes a splitting of the line due to the second-order recoupling of the chemical-shielding and the dipolar-coupling tensors. A similar effect is well known in liquid-state NMR as off-resonance decoupling, where an apparently scaled J coupling is obtained by off-resonance irradiation of a coupled heteronuclear two-spin system.[15,16] However, in that case all the quantities (J coupling and resonance offset) are scalar. The fact that both the dipolar coupling and the chemical shielding are second-rank tensors has new and interesting consequences. The second-order recoupling of the two tensors shows also very different properties compared to the off-resonance cw decoupling in solid-state NMR. Off-resonance decoupling in solids results in a coupling of the scalar isotropic resonance offset and the second-rank dipolar-coupling tensor which results in a purely second-rank interaction. This second-rank tensor is averaged out under MAS conditions.

The product of two second-rank tensors can generally be described by a weighted sum of a zeroth-rank, a second-rank, and a fourth-rank tensor.[27] To decompose the tensor product into a sum of tensors and calculate the influence of single-axis rotation on the different components, we have to consider the transformations of both tensors from their respective principal-axis systems (PAS) into the laboratory-fixed coordinate system (Fig. 2). The chemical-shielding tensor is first rotated into the PAS system of the dipolar-coupling tensor. Then both the chemical-shielding tensor and the dipolar-coupling tensor are rotated into the rotor-fixed frame from which they are subsequently rotated into the laboratory-fixed coordinate system. This leads to the following time-dependent transformation for the two tensors:

$$\omega_D(\Omega,t)=\frac{1}{\sqrt{6}}\sum_{n=2}^{-2}\mathscr{D}^2_{n,0}(\omega_r t,\beta_r,0)\times\mathscr{D}^2_{0,n}(\alpha,\beta,\gamma)\cdot\rho^D_{2,0}, \tag{11}$$

$$\omega_I(\Omega,t)=\frac{2}{\sqrt{6}}\sum_{m=-2}^{2}\sum_{m'=-2}^{2}\sum_{m''=-2}^{2}\mathscr{D}^2_{m,0}(\omega_r t,\beta_r,0)\times\mathscr{D}^2_{m',m}(\alpha,\beta,\gamma)\mathscr{D}^2_{m'',m'}(\alpha_I,\beta_I,\gamma_I)\cdot\rho^I_{2,m''}. \tag{12}$$

The Wigner rotation-matrix elements $\mathscr{D}^2_{m,n}(\alpha,\beta,\gamma)$ are defined according to Ref. 27, and β_r is the inclination angle of

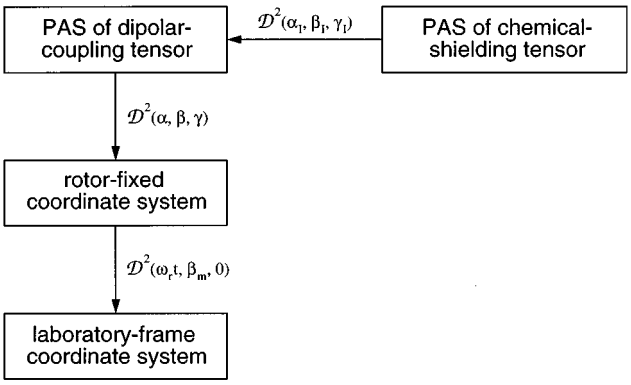

FIG. 2. Sequence of transformations and Euler angles necessary to rotate the two tensors from their respective principal-axis systems into the laboratory-fixed coordinate system. The chemical-shielding tensor is first rotated into the principal-axis system of the dipolar coupling tensor ($\mathscr{D}^2(\alpha_I,\beta_I,\gamma_I)$), and then both tensors are rotated into the rotor-fixed frame ($\mathscr{D}^2(\alpha,\beta,\gamma)$) and from there finally into the laboratory-fixed frame ($\mathscr{D}^2(\omega_r t,\beta_m,0)$).

the rotation axis to the static magnetic field. The sample spinning frequency is ω_r, and Ω is the full set of Euler angles necessary to describe all transformations. The set of angles (α,β,γ) describes the orientation of a selected crystallite (powder average), and $(\alpha_I,\beta_I,\gamma_I)$ are the three Euler angles describing the orientation of the I-spin chemical-shielding tensor in the principal-axis system of the dipolar-coupling tensor. The dipolar-coupling tensor is always axially symmetric and is defined in its principal-axis system as[2]

$$\rho^D_{2,0} = \sqrt{\frac{3}{2}} \cdot \delta_D . \tag{13}$$

The chemical-shielding tensor components in their PAS are given by[2]

$$\rho^I_{2,0} = \sqrt{\frac{3}{2}} \cdot \delta_I ,$$
$$\rho^I_{2,\pm 2} = \frac{1}{2} \cdot \eta_I \delta_I . \tag{14}$$

The parameters δ_D, δ_I, and η_I are defined as in Eqs. (2) and (3). We are interested in the time-averaged transition frequencies given by

$$\omega_{3,4}(\Omega) = \langle \omega_{3,4}(\Omega,t) \rangle_{\beta_r} \approx \left\langle \omega_S(\Omega,t) \pm \left\langle \frac{\omega_D(\Omega,t)\omega_I(\Omega,t)}{\omega_{\rm rf}} \right\rangle \right\rangle_{\beta_r} , \tag{15}$$

where $\langle \cdots \rangle_{\beta_r}$ represents the time average over a full rotor period. Equation (15) only has nonvanishing contributions under the condition $m=-n$, where m and n are the summation indices from Eqs. (11) and (12). Under this condition, Eq. (15) can be substantially simplified, and one obtains the following result for the time-averaged transition frequencies:

$$\begin{aligned}\omega_{3,4}(\Omega) = \sqrt{\frac{2}{3}}\, d^2_{0,0}(\beta_r) \sum_{m'=-2}^{2} \mathscr{D}^2_{m',0}(\alpha,\beta,0) \\ \times \sum_{m''=-2}^{2} \mathscr{D}^2_{m'',m'}(\alpha_S,\beta_S,0)\cdot \rho^S_{2,m''} \pm \frac{1}{3\omega_{\rm rf}} \cdot \rho^D_{2,0} \\ \cdot \sum_{j=0,2,4} C(2,2,j;0,0)\cdot d^j_{0,0}(\beta_r) \\ \times \sum_{m'=-2}^{2} \mathscr{D}^j_{m',0}(\alpha,\beta,0)\cdot C(2,2,j;0,m') \\ \times \sum_{m''=-2}^{2} \mathscr{D}^2_{m'',m'}(\alpha_I,\beta_I,0)\cdot \rho^I_{2,m''} .\end{aligned} \tag{16}$$

Here, $C(j_1,j_2,j;m_1,m_2)$ are Clebsch–Gordan coefficients as defined in Ref. 28 and $d^j_{m,n}(\beta)$ are reduced Wigner rotation matrix elements.[27] Equation (16) shows that we indeed obtain the sum of three different terms ($j=0,2,4$) which scale as a zeroth-rank, a second-rank, and a fourth-rank tensor under single-axis rotation. Setting the angle of the rotation axis to $\beta_r=0°$ gives the solution for the static spectrum. If the inclination angle of the rotation axis to the static magnetic field corresponds to the magic angle ($\beta_r=54.74°$), all second-rank contributions to the transition frequencies will vanish. The chemical-shielding tensor of the S spin and the second-rank contribution to the second-order term are scaled to zero, and only an isotropic part and a scaled fourth-rank tensor part remain. They give rise to an isotropic splitting of the line described by the zeroth-rank tensor part of Eq. (16) and an additional orientation-dependent splitting described by the fourth-rank tensor contribution. It is possible to average out both the second-rank and the fourth-rank tensor components of Eq. (16) simultaneously by using dynamic-angle spinning (DAS) or double rotation (DOR).[12–14] In this case the resulting second-order coupling is fully isotropic and gives rise to a spectrum that consists of a sharp doublet.

Equation (16) allows very efficient simulation of the second-order recoupled spectra which is important if extraction of parameters from measured spectra is desired. Nonlinear least-square fitting to obtain parameters (orientation of the two tensors) and their corresponding error ranges is possible based on the analytical solution. The result of Eq. (16) agrees with our previous analytical result obtained for the coupling of the dipolar-coupling tensor with itself as observed in the isotropic second-order dipolar shift, assuming $\eta_I=0$ and setting the angle between the two tensors to zero ($\beta_I=0$).[21]

Although the second-order recoupling contains interesting information concerning the orientation of the two tensors, it is sometimes desirable to remove the splitting to obtain a single sharp line for each resonance. The simplest way to calculate the Hamiltonian under a multiple-pulse sequence is to use average Hamiltonian theory.[1,29] For cw decoupling with the rf field along the x axis the average Hamiltonian to first order is given by

$$\bar{\mathscr{H}}^{(0)} = \omega_S(\Omega_S)\cdot S_Z \tag{17}$$

and

$$\bar{\mathscr{H}}^{(1)}=\frac{\omega_D(\Omega_D)^2+\omega_I(\Omega_I)^2}{2\omega_{\rm rf}}I_X+\frac{\omega_D(\Omega_D)\omega_I(\Omega_I)}{\omega_{\rm rf}}\cdot 2I_XS_Z. \tag{18}$$

The first term of Eq. (18) is the second-order isotropic dipolar shift which we have previously analyzed and discussed.[21] Since the first term commutes with the S-spin subspace of the density operator it has no influence on the time evolution of the S spin. The second term describes the second-order recoupling of the chemical-shielding and dipolar-coupling tensors. In the limit of strong decoupling, the result from average Hamiltonian theory is fully equivalent to the result derived from second-order static perturbation theory [Eq. (10)] and illustrates the fact that the first-order average Hamiltonian corresponds to second-order static perturbation theory.[30] The problem of folded decoupling sidebands[6] is not relevant in our case since we analyze only the main transitions [Eq. (6)] and have neglected the minor ones [Eq. (5)]. Such a treatment is justifiable in the limit of strong decoupling because the intensities of the minor transitions are very small under this condition [Eqs. (7) and (8)]. Using the well known fact that symmetric pulse sequences eliminate all odd orders of the average Hamiltonian[1] we can easily design very simple pulse sequences to remove the second-order recoupling term (first-order average Hamiltonian). The simplest such experiment consists of alternating $(2\pi)_{+x}$ and $(2\pi)_{-x}$ pulses. However, all multiple-pulse sequences used in high-resolution liquid-state NMR also fulfill the symmetry condition and could possibly be used. Under MAS the length of the pulse sequence is an important consideration. The repetition rate of the sequence should be considerably faster than the mechanical spinning speed of the sample to avoid interferences between the two different averaging processes.[31–33] The phase-alternating sequence and other simple symmetric sequences will be experimentally analyzed and discussed in Sec. III.

The reason that the second-order recoupling of the dipolar-coupling and the chemical-shielding tensors is not as prominent in normal solids is the strong homonuclear dipolar-coupling network among the protons. The spin flip–flop terms of the homonuclear dipolar-coupling Hamiltonian lead to an additional modulation of the heteronuclear dipolar coupling which results in a narrowing of the lines of the decoupled heteronuclear spin (''self-decoupling'').[2,17,34] If the decoupling field is applied off resonance, such that the effective field is inclined at an angle φ_I to the static magnetic field, we obtain the following effective homonuclear dipolar-coupling Hamiltonian in the tilted rotating frame:[1]

$$\bar{\mathscr{H}}_{II}^{(0)}=P_2(\cos\,\varphi_I)\cdot\sum_{k<m}\omega_D^{(k,m)}(\Omega_D^{(k,m)})\times(3I_{kz}I_{mz}-\mathbf{I}_k\cdot\mathbf{I}_m). \tag{19}$$

The homonuclear dipolar coupling scales like a second-rank spin tensor, and thus for $\varphi_I=54.74°$ (magic angle) Equation (19) is zero. The vanishing homonuclear dipolar-coupling Hamiltonian leads to a broadening of the line of the decoupled heteronuclear spin because the second-order recoupling is no longer quenched by the homonuclear spin flip–flop terms. Such a line broadening for an effective decoupling field along the magic angle has been observed experimentally.[2,4,35–37] Off-resonance decoupling with the effective field inclined at the magic angle also scales the heteronuclear dipolar coupling in the tilted-rotating frame

$$\bar{\mathscr{H}}_{IS}^{(0)}=\cos\,\varphi_I\cdot\omega_D(\Omega_D)\cdot 2I_zS_z. \tag{20}$$

This scaled zero-order contribution to the broadening is purely second rank and, assuming that the sample spinning is fast enough, will be averaged out by MAS.

It has been observed experimentally that in ferrocene, where the homonuclear dipolar couplings are scaled and weak due to fast internal motion, the ^{13}C linewidth of the proton-decoupled spectrum under MAS increases with increasing MAS spinning speed.[5] This phenomenon can be qualitatively understood in the framework of the second-order recoupling. At low spinning speeds the quenching of the second-order recoupling by the homonuclear proton–proton dipolar coupling is still efficient. At higher spinning speeds the homonuclear dipolar-coupling network is weakened and the self-decoupling effect is reduced resulting in a broadening of the line of the decoupled spin.

As can be seen from the widespread use of cw decoupling under MAS the second-order recoupling is not as apparent in solids with strong homonuclear dipolar couplings as it is in isolated two-spin systems. Recently a new decoupling scheme for solids under MAS conditions called ''two pulse phase modulation'' (TPPM)[7] has been published which significantly reduces the linewidth compared to cw decoupling. The sequence consists of pulses with flip angles β and alternating phases $\pm\varphi$. Numerical simulations and experiments have shown that the optimum flip angle and phase depend on the spinning speed but are usually around $\beta\approx 180°$ and $\varphi\approx 20°$. Such a sequence can be viewed as a strong cw decoupling field along the x axis with a small phase-alternating field along the y axis superimposed on it. The strong cw decoupling field is necessary because of the strong homonuclear dipolar couplings while the small phase-alternating field reduces the second-order recoupling effects. We would like to emphasize that the resonance offset is not sufficient to explain the broadening observed in the spectra presented here. The interference between the dipolar-coupling tensor and the resonance offset term leads to a purely second-rank second-order contribution to the line broadening which would be averaged out by magic-angle sample spinning. Using average Hamiltonian calculations for the following model pulse sequence $(180^{\circ}_{+\varphi},180^{\circ}_{-\varphi})_N$ with $\varphi=\pi/(2N)$ we can show why the TPPM decoupling scheme leads to a reduction of the second-order recoupling term. The above choice of φ and N ensures that the sequence is cyclic in the average Hamiltonian sense. The zeroth-order and first-order average Hamiltonians can be calculated for the general sequence with $N>1$ leading to

$$\bar{\mathscr{H}}^{(0)}=\omega_S(\Omega_S)\cdot S_Z \tag{21}$$

and

$$\bar{\mathscr{H}}^{(1)}=\frac{2\tan\varphi}{\pi}\cdot\left[\frac{\omega_D(\Omega_D)^2+\omega_I(\Omega_I)^2}{2\omega_{\rm rf}}\cdot I_Z+\frac{\omega_D(\Omega_D)\omega_I(\Omega_I)}{\omega_{\rm rf}}\cdot 2I_ZS_Z\right]. \tag{22}$$

Based on Eq. (22) we can predict that the residual line width should decrease with decreasing phase φ. However, as φ decreases the number of pulse-sequence cycles N needed to obtain the full averaging increases, and one has to find an optimum condition which satisfies the goal of a narrow line and avoids interference between the pulse sequence and the mechanical sample rotation. Comparing Eq. (22) with the equivalent result for cw decoupling [Eq. (18)] shows that the residual second-order coupling obtained under the TPPM sequence is $2\cdot\tan(\varphi)/\pi$ smaller than for cw decoupling. For $\varphi=20°$ this is 0.23 or more than a factor of 4 in reduction of the second-order recoupling contribution to the line broadening. Despite the simplifications made in the derivation of the average Hamiltonian, Eq. (22) illustrates why the TPPM decoupling scheme works and how it is connected with the second-order recoupling of the dipolar-coupling and the chemical-shielding tensors.

All theoretical calculations shown so far are based on the assumption that the decoupling field strength $\omega_{\rm rf}$ is greater than the maximum value of both tensors and much larger than the MAS spinning speed. If the second assumption is not true, the consecutive averaging approach used in our calculations breaks down, and we have to use different methods to predict the spectrum. One possibility is the use of rotor-synchronized rf irradiation as has been done in the analysis of ''rotary resonance recoupling'' (R^3).[22–25] However, for long cycle times $(2\pi/\omega_r)$ the question of the convergence of the average Hamiltonian series arises,[38,39] and it might be necessary to calculate higher orders of average Hamiltonian.

III. EXPERIMENTAL RESULTS

All experiments were performed on a home-built spectrometer operating at a proton Larmor frequency of 301.2 MHz. A commercial 4 mm MAS probe assembly from Chemagnetics was used for the MAS experiments, and a home-built variable-angle probe[12,40] with a Doty Scientific 7 mm spinning module was used for the DAS experiments. The spinning frequency was controlled by a home-built spinning-speed controller (MAS probe only). As a model substance for an isolated two spin system (^{1}H–^{15}N), we used fully ^{15}N labeled tri-(trideuteromethyl)-ammoniumchloride. The shortest nitrogen–nitrogen distance calculated from the crystallographic data of trimethylammoniumchloride[41] is 5.7 Å corresponding to a dipolar-coupling constant of $\delta_D/(2\pi)=13.3$ Hz. The shortest proton–proton distance is of the same order of magnitude. The dipolar coupling of the ^{15}N–^{1}H spin pair was measured from static and slow-spinning MAS spectra and was found to be $\delta_D/(2\pi)=20\,110\pm206$ Hz corresponding to a distance of $r_{\rm NH}=1.066\pm0.004$ Å. The chemical-shielding tensor of ^{15}N in this compound is very small. A static proton-decoupled spectrum (data not shown) using a symmetric $(2\pi)_{+x}$, $(2\pi)_{-x}$ sequence resulted in a Gaussian line with a half width at half height of 290 Hz. The chemical-shielding tensor of the proton was not measured directly. Its anisotropy was obtained from fitting the second-order MAS spectrum assuming that the PAS of the chemical-shielding tensor of the proton and the PAS of the dipolar-coupling tensor are coaxial. The value obtained from these fits was $\delta_I/(2\pi)=6800\pm200$ Hz. This value agrees with independent measurements of the chemical-shielding tensor.[42]

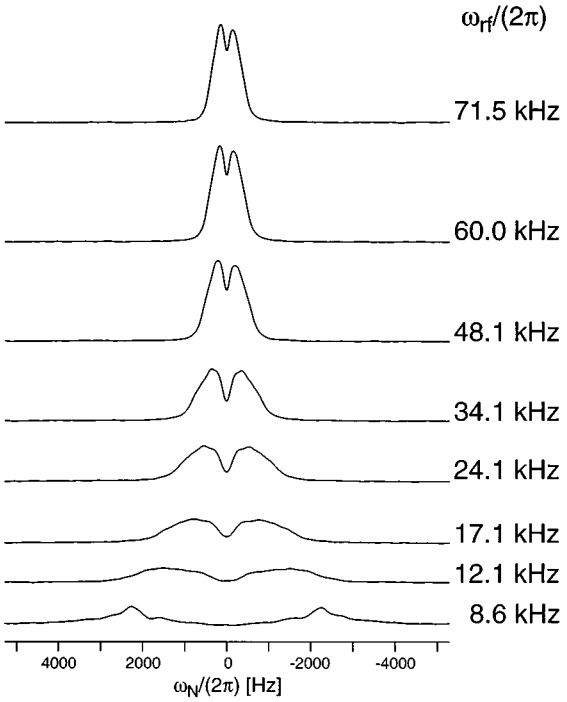

FIG. 3. ^{15}N spectra of ^{15}N-labeled tri-(trideuteromethyl)-ammoniumchloride as a function of the proton decoupling power. The decoupling field strength was varied from $\omega_{\rm rf}/(2\pi)=8.6$ kHz to $\omega_{\rm rf}/(2\pi)=71.5$ kHz. Even for the highest decoupling power the line is still split and rather broad. The full width of the line scales linearly with the inverse of the decoupling field strength, as expected.

The experiments under magic-angle sample spinning were performed using a standard cross-polarization sequence with cw decoupling during the acquisition.[43–45] Figure 1 shows 1D spectra without (a) and with (b) decoupling of the protons by cw irradiation. The spectrum without decoupling [Fig. 1(a)] shows a single sharp line with spinning side bands, while the spectrum with decoupling [Fig. 1(b)] shows a split and broadened line. Figure 3 shows a series of ^{15}N spectra where the proton-decoupling field strengths was varied from $\omega_{\rm rf}/(2\pi)=8.6$ kHz to $\omega_{\rm rf}/(2\pi)=71.5$ kHz. The spectra were recorded with a CP contact time of 0.5 ms and a MAS spinning speed of $\omega_r/(2\pi)=5$ kHz. Two hundred and fifty-six time points were recorded and 1024 scans were added up for each of the experiments. Even with the highest decoupling field strength we see a rather large broadening as well as a splitting. Both the splitting and the broadening are due to the zeroth-rank and fourth-rank tensor contributions to the second-order recoupling since MAS can only average out

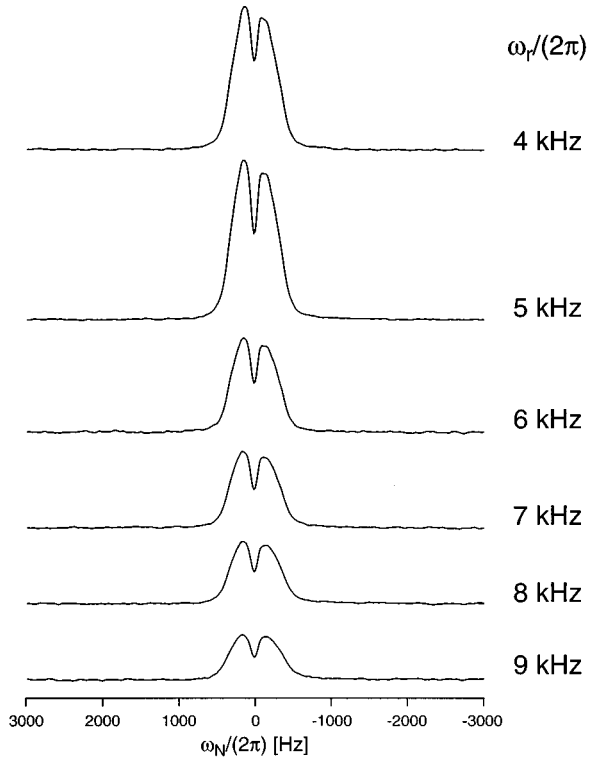

FIG. 4. ^{15}N spectra under cw proton decoupling for six different MAS spinning speeds from $\omega_r/(2\pi)=4$ kHz to $\omega_r/(2\pi)=9$ kHz. The decoupling field strength in all spectra was set to $\omega_{rf}/(2\pi)=71.5$ kHz. The width of the line is independent of the MAS spinning speed. The variation in the line intensities is due to varying cross-polarization efficiency at different spinning speeds.

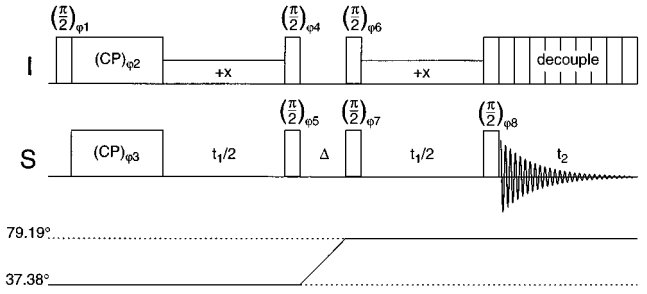

FIG. 5. Pulse sequence used to measure the DAS spectrum of the second-order recoupling. The pulse sequence implements pure phase during t_1 (Ref. 47) by storing the appropriate orthogonal components during the change of the rotor axis and adding up two data sets modulated as $\cos^2(\omega t_1/2)$ and $\sin^2(\omega t_1/2)$. The rf field strength during the two decoupling periods must be equal. The phase cycle was as follows (phases are given in multiples of 90 deg, φ_R is the receiver phase): φ_1: 0 2; φ_2: 1 3; φ_3 and φ_8: 0 0 1 1 2 2 3 3; φ_4: 1; φ_5 and φ_7: 0 0 1 1 2 2 3 3 3 3 0 0 1 1 2 2; φ_6: 3; φ_R: 2 0 3 1 0 2 1 3. To record the second data set needed for States-type processing in t_1 the phase of φ_3 was shifted by 90° while keeping the phase of all other pulses and the receiver unchanged.

the second-rank tensor component. The line width of the spectra at different decoupling powers correlate very well (correlation coefficient $R=0.998$) with the inverse of the proton-decoupling field strength as expected from the theoretical calculations shown in Sec. II. This shows that we are justified in neglecting all terms higher than second order in the expansion of Eq. (9).

In order to investigate the influence of the spinning speed on the second-order recoupling and to rule out rotational-resonance phenomena[22–25] as the source of the observed splitting, we recorded cw-decoupled spectra as a function of the spinning speed from $\omega_r/(2\pi)=4$ kHz to $\omega_r/(2\pi)=9$ kHz with an rf field strength of $\omega_{rf}/(2\pi)=71.5$ kHz (Fig. 4). The spectra are unchanged over the full range of spinning speeds except for an overall decrease in intensity with increasing spinning speed. The decrease in intensity is explained by the lower cross-polarization efficiency at higher spinning speeds since standard Hartmann–Hahn cross polarization was used rather than one of the newer methods designed to achieve efficient cross polarization while spinning at the magic angle.[46] If a quantitative analysis of the second-order powder pattern is of interest one has to make sure that the cross-polarization process does not favor certain crystallite orientations.

As mentioned already in Sec. II, the second-order recoupling can be made isotropic by performing the experiment under DOR or DAS conditions. The pulse sequence used to record an isotropic second-order recoupled spectrum under DAS is shown in Fig. 5. The experiment is implemented as a pure-phase experiment[47] in t_1 and uses States-type processing[48] in ω_1 to distinguish between positive and negative frequencies. Since the second-order recoupled Hamiltonian is quantized along the decoupling field for the I spins [Eq. (18)], additional storage pulses for the I spins before and after the change of the rotor axis are needed compared to a standard pure-phase DAS experiment.[47]

For the 2D-DAS experiment 50 t_1 times were recorded with 256 scans of 256 points in t_2 for each of the two complex data sets. During t_2, phase-alternating 2π-pulse decoupling (see next paragraph) was employed to obtain a narrow line in ω_2. The flipping time to change the angle from $\beta_1=37.38°$ to $\beta_2=79.19°$ was set to $\Delta=100$ ms. During this time no noticeable loss of magnetization was observed since the longitudinal relaxation times of both spins are considerably longer than Δ. The rf field strength during the cw decoupling in t_1 was $\omega_{rf}/(2\pi)\approx 35.7$ kHz. After a hypercomplex Fourier transformation and phase correction, a slice through the highest point in ω_2 along ω_1 was taken and is shown in Fig. 6. A comparison with a MAS spectrum recorded under similar conditions shows a significant narrowing of the line due to the simultaneous averaging of the second-rank and fourth-rank tensors. However, the DAS spectrum still has very broad lines which may be due to inaccuracies in adjusting the two DAS angles or differences in the cw-decoupling field strengths at the two different rotor orientations. The splitting obtained by a fit of the DAS spectrum to two Lorentzian lines is $\Delta\omega=650\pm100$ Hz. It would be advantageous to implement this experiment under DOR instead of DAS. Both problems, the adjustment of the two angles and the differences in the rf field strengths, would not be present under DOR.

As pointed out in the previous section, we can eliminate

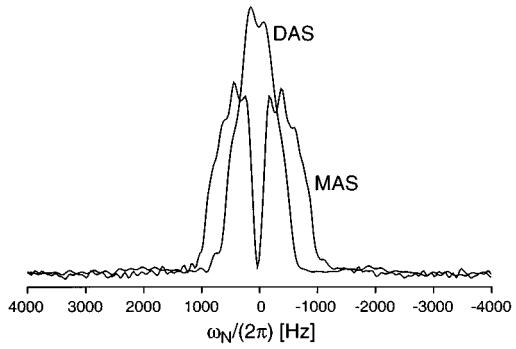

FIG. 6. Magic-angle sample spinning (MAS) and dynamic-angle sample spinning (DAS) spectra for a decoupling field strength of $\omega_{rf}/(2\pi)=35.7$ kHz. The MAS spectrum was recorded as a 1D cross-polarization cw-decoupling spectrum, while the DAS spectrum was recorded with the pulse sequence of Fig. 5. The 1D spectrum shown is the slice through the highest point in ω_2 along the ω_1 dimension. The DAS spectrum is considerably narrower due to the simultaneous averaging of second-rank and fourth-rank tensor contributions. The splitting of the two lines in the DAS spectrum corresponds to the isotropic value of the second order recoupling of the chemical-shielding and the dipolar-coupling tensors.

the second-order effects in the rotating frame by using a symmetric decoupling sequence instead of cw irradiation. The simplest implementation of such a sequence is a phase alternating $(2\pi)_{+x}$, $(2\pi)_{-x}$ decoupling sequence. Figure 7 shows a series of 1D spectra obtained with this type of synchronous phase-alternating decoupling with an rf field strength of $\omega_{rf}/(2\pi)=71.5$ kHz. The line is sharp with a half width at half height of $\Delta\omega/(2\pi)\approx 45$ Hz and varies only slightly over the range of spinning speeds ($\omega_r/(2\pi)=4$ kHz to $\omega_r/(2\pi)=9$ kHz). The decreasing intensity of the line is again due to the lower efficiency of the cross polarization at higher spinning speeds. Other simple decoupling schemes (MLEV-4[49,50] and WALTZ-4[51,52]) have also been implemented and give slightly narrower lines with $\Delta\omega/(2\pi)\approx 30$ Hz at slow spinning speeds. However, at higher spinning speeds interference effects between the pulse sequence and the mechanical sample spinning appear. They lead to a broadening of the line and give rise to sidebands (data not shown). Such interference between two averaging processes that are not synchronized is a well known effect which has been described in the literature.[31–33]

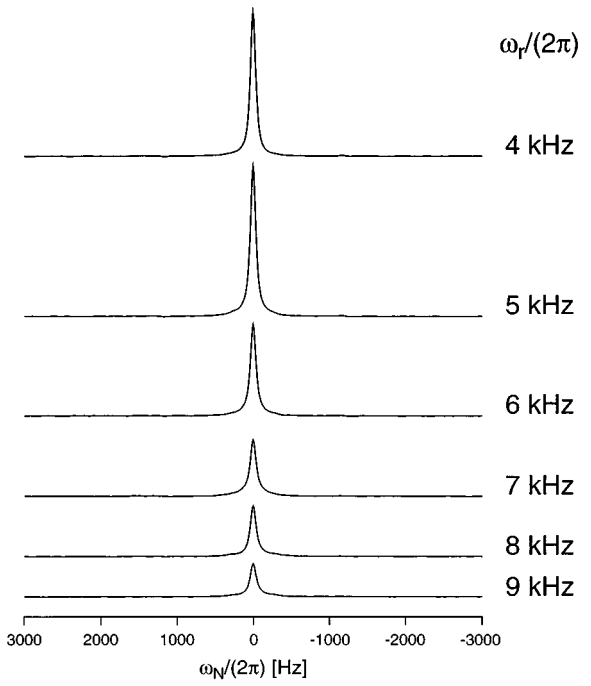

FIG. 7. ^{15}N spectra under proton decoupling using a phase alternating $(2\pi)_{+x'}$ $(2\pi)_{-x}$ sequence. The half width at half height of the line is 45 Hz and is independent of the spinning speed. The variation in the line intensity is due to varying cross-polarization efficiency at different spinning speeds.

IV. NUMERICAL SIMULATIONS

In order to illustrate some of the features of the second-order recoupling of the chemical-shielding and the dipolar-coupling tensors we have performed numerical simulations using the parameters of our model compound. The simulations were performed using the NMR simulation environment GAMMA.[53] In all simulations the dipolar-coupling tensor was set to $\delta_D/(2\pi)=20$ kHz and the chemical-shielding tensor was assumed to be axially symmetric ($\eta_I=0$) with an asymmetry of $\delta_I/(2\pi)=6.8$ kHz.

The accuracy of simulations based on the analytical solution from second-order perturbation theory [Eq. (16)] was tested by comparing exact numerical simulations calculated by small step integration of the time-dependent Hamiltonian with simulations based on the analytical solution at different rf field strengths. The numerical simulations were done for an MAS frequency of $\omega_r/(2\pi)=5$ kHz and with 5000 time steps per rotor cycle leading to a 40 ns time resolution. The two tensors were assumed to be coaxial. Simulations for 300 different crystallite orientations were added up using the method of Cheng *et al.*[54] to obtain optimum coverage of the sphere. The dwell time was set to one third of the rotor cycle (SW=15 kHz) and 4096 data points were computed. The spectra were processed with a line broadening of 100 Hz. The spectra based on the analytical solution of the time-averaged Hamiltonian were calculated in the frequency domain. All parameters were the same as in the time-domain simulations except that 10 000 different powder orientations were added up. The resulting frequency-domain spectra were convolved with a 100 Hz Lorentzian line. The spectra calculated by the two different methods for three different rf field strengths $\omega_{rf}/(2\pi)=70$, 30, and 10 kHz are shown in Fig. 8. The time-domain spectra show spinning sidebands at ± 5 kHz. It is apparent that for the two higher rf field strengths the two simulation methods agree very well with differences in the central line on the order of 1%. The small deviations could be due to the finite time steps in the time-domain simulations, the truncation of the analytical solution in second order, or the different number of powder points used in the two simulation methods. However, they are so small that they can be neglected. For $\omega_{rf}/(2\pi)=10$ kHz, the differences are very large and the shape of the two spectra is very different. This is due to the breakdown of the assumptions made

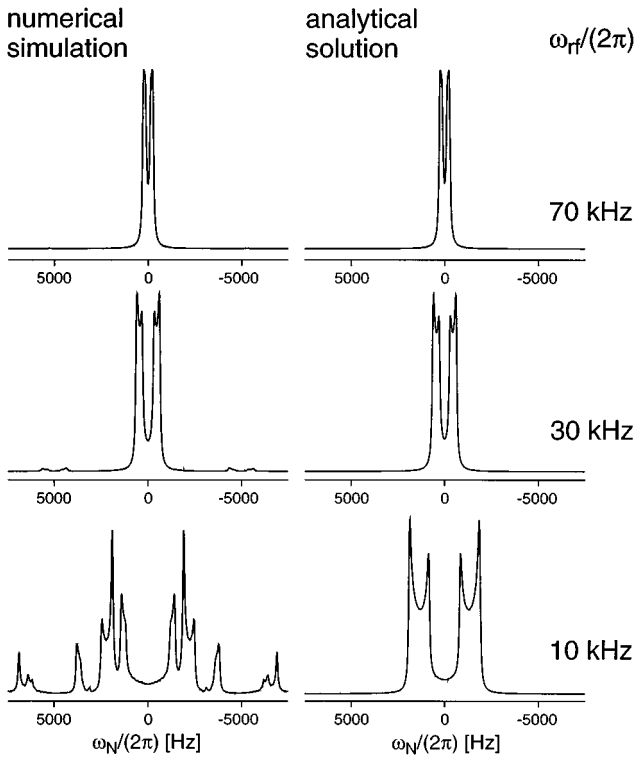

FIG. 8. Comparison of simulations based on small-step numerical integration of the time-dependent Hamiltonian and simulations based on the analytical solution of Eq. (16) for three different decoupling field strength. The two simulations at $\omega_{rf}/(2\pi)=70$ and 30 kHz show differences on the order of 1%. The simulations at $\omega_{rf}/(2\pi)=10$ kHz are very different which reflects the fact that the assumptions made in the second-order truncation [Eq. (9)] are not valid here. The parameters used for the simulations were $\delta_D/(2\pi)=20$ kHz, $\delta_I/(2\pi)=6.8$ kHz, and $\eta_I=0.0$. The spinning speed was $\omega_r/(2\pi)=5$ kHz for the time-domain simulations which is reflected in the spinning sidebands at 5 kHz. The two tensors were assumed to be coaxial ($\beta_I=0°$).

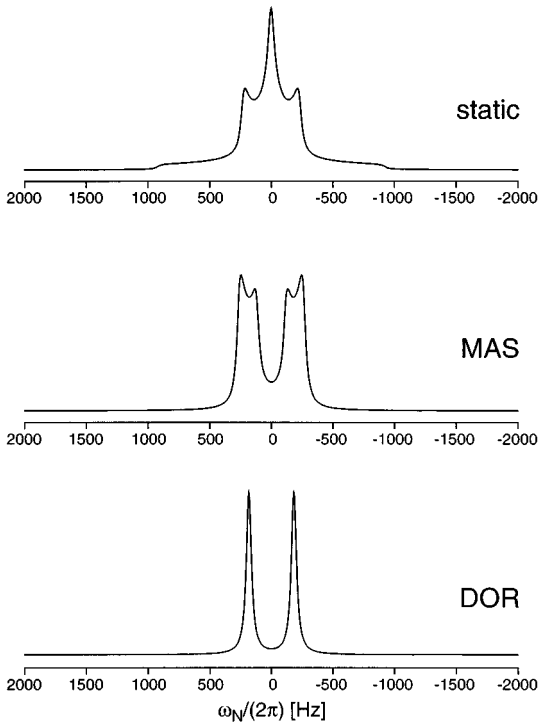

FIG. 9. Simulated second-order recoupled spectra under static, magic-angle sample spinning, and double rotation conditions showing the averaging properties of the second-order Hamiltonian. The static spectrum is very broad (full width 1838 Hz) and shows a superposition of a zeroth-rank, a second-rank, and a fourth-rank tensor contribution to the Hamiltonian. The MAS spectrum is a pure fourth-rank tensor powder pattern superimposed on an isotropic splitting with a full width of 528 Hz. The DOR spectrum shows only the isotropic splitting of 363 Hz. The dipolar coupling constant was $\delta_D/(2\pi)=20$ kHz; the chemical-shielding tensor parameters were $\delta_I/(2\pi)=6.8$ kHz and $\eta_I=0.0$; and the two tensors were assumed to be coaxial ($\beta_I=0°$). The rf field strength was $\omega_{rf}/(2\pi)=71.5$ kHz.

in deriving the analytical solution in Eq. (9). At an rf field strength of 10 kHz the decoupling field strength is no longer greater than the magnitudes of the chemical-shielding and the dipolar-coupling tensors. Figure 8 illustrates that the truncation in second order is a good approximation as long as the decoupling field strength is larger than the maximum value of the two tensors as it is required for the validity of Eq. (9). The advantage of the frequency-domain simulation based on the analytical solution is its speed. The frequency-domain simulation is 6000 times faster than the time-domain simulation using small step integration of the Liouville–von Neumann equation. The frequency-domain simulation using 10 000 different crystallite orientations took only 17 s cpu time on a SGI Indigo with an 100 MHz MIPS R4000 processor.

Figure 9 shows the second-order recoupled spectra under static, magic-angle sample spinning, and double rotation conditions illustrating the averaging properties of the second-order recoupled Hamiltonian under spatial rotation. The simulations were performed as frequency-domain simulations based on the analytical solution shown in Eq. (16). Again, the two tensors were assumed to be coaxial and the decoupling field strength was $\omega_{rf}/(2\pi)=71.5$ kHz. Ten thousand different crystallite orientations were added up, and the resulting spectrum was convolved with a Lorentzian linewidth of 50 Hz. The static spectrum is very broad with a full width of 1838 Hz. It is the result of a superposition of the isotropic splitting with the second-rank and the fourth-rank contributions to the second-order Hamiltonian. The MAS spectrum shows a pure fourth-rank tensor powder pattern superimposed on the isotropic splitting with a full width of 528 Hz. The DOR spectrum shows, as expected, two sharp lines with an isotropic splitting of 363 Hz.

The dependence of the second-order recoupled spectra on the relative orientation of the two tensors is illustrated in Fig. 10. The simulations were done as frequency-domain simulations using the same parameters as for the spectra shown in Fig. 8. It can be seen that there is a strong dependence of the line shape on the angle β_I as expected from Eq. (16). It is not straightforward to predict the line shape from Eq. (16) especially if the chemical-shielding tensor is not axially symmetric. The simulations of Fig. 10, however, show that the variations should be strong enough to allow the

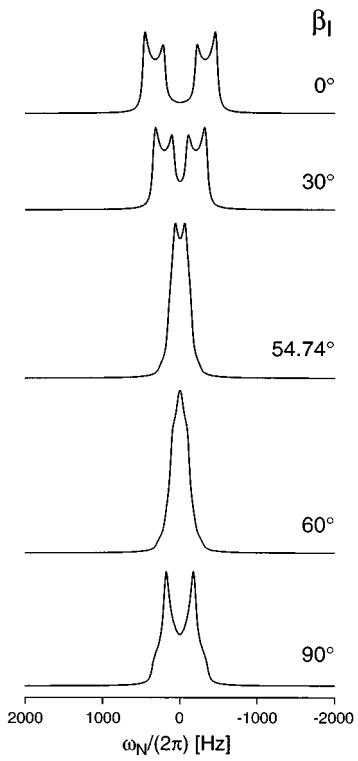

FIG. 10. Dependence of the second-order recoupled spectrum on the orientation of the two tensors. The chemical shielding tensor was assumed to be axially symmetric so only one parameter (β_I) is needed to describe the orientation of the principal-axis systems of the two tensors. The line shape of the spectrum depends very strongly on this angle which suggests that it might be possible to determine the angle between the two tensors from experimental spectra. The parameters of the simulation are the same as in Fig. 9.

determination of the angle between the two tensors from this type of second-order spectrum.

We have developed a program which allows the simultaneous optimization of the following seven parameters: asymmetry of the dipolar-coupling tensor (δ_D), asymmetry and anisotropy of the chemical-shielding tensor (δ_I and η_I), two Euler angles (α_I and β_I), the line broadening, and the isotropic chemical shift of the S spin (ω_S^{iso}). It is based on the frequency-domain simulations using the analytical solution of Eq. (16) and uses nonlinear least-square fitting to obtain the optimum parameters and error estimates. It is obvious that a simultaneous optimization of all seven parameters does not make sense due to the high correlations between some of the parameters. We have used this program to obtain a value for the anisotropy of the chemical-shielding tensor from the second-order MAS spectrum of Fig. 3. Three parameters (δ_I, ω_S^{iso}, and the line broadening) were optimized simultaneously assuming that the I-spin chemical-shielding tensor is axially symmetric ($\eta_I=0.0$) and that the two tensors are coaxial ($\beta_I=0°$). The value obtained from these fits is $\delta_I/(2\pi)=6800\pm200$ Hz. So far we have not explored the possibilities to use the second-order MAS spectra to obtain the orientation of the principal-axis systems of the two tensors.

V. CONCLUSIONS

We have shown that the second-order recoupling of the dipolar-coupling and the chemical-shielding tensors is an important source of residual line broadening in cw-decoupled spectra of isolated two-spin systems. Since this residual broadening results from the coupling of two second-rank tensors it will not average out under MAS conditions because of the zeroth-rank and fourth-rank tensor contributions. In the case of our model system (^{1}H–^{15}N) we have seen broadenings of ca. 1000 Hz for a decoupling field of $\omega_{\mathrm{rf}}/(2\pi)=71.5$ kHz. The use of a simple phase-alternating sequence which is symmetric in the sense of the average Hamiltonian theory removes the second-order broadening in spin systems with weak homonuclear dipolar-coupling networks. In spin systems with strong homonuclear dipolar-coupling networks, the second-order recoupling is also contributing to the residual line broadening. The use of the TPPM decoupling scheme[7] leads to a reduced second-order broadening even in solids with strong homonuclear dipolar-coupling networks.

The impact of this second-order recoupling will most visibly be seen in doubly labeled substances which are now more commonly used in the structure determination of peptides and proteins by solid-state NMR. We can estimate the magnitude of the broadening for a ^{13}C–^{15}N double label based on the analytical results of Eq. (16). Calculating for a one bond distance, a carbon chemical-shielding tensor of $\delta/(2\pi)=9750$ Hz (78 ppm at 125 MHz carbon larmor frequency), and a decoupling field strength of 70 kHz one obtains a residual linewidth of approximately 200 Hz.

It is possible to use the second-order recoupling to extract information about the magnitude or the orientation of the principal-axis systems of the two interfering tensors from the second-order spectrum. In systems with strongly dipolar-coupled protons, the use of off-resonance decoupling, with the effective decoupling field along the magic angle, can reduce the quenching of the second-order recoupling by the homonuclear flip–flop modulations. Such off-resonance decoupling might allow the extraction of structural information from the second-order recoupled spectra even in systems with strong homonuclear dipolar-coupling networks. Further investigations in this direction are under way in our laboratory.

ACKNOWLEDGMENTS

This work was supported by the Director, Office of Energy Research, Office of Basic Energy Sciences, Materials Sciences Division, U.S. Department of Energy, under Contract No. DE-AC03-76SF00098. We are indebted to Herbert Zimmermann for synthesizing the ^{15}N labeled and fully deuterated trimethylammoniumchloride. Many stimulating and helpful discussions with Dr. Matthew Augustine and experimental support by Jonathan Heller are gratefully acknowledged. We would also like to thank Susan De Paul for carefully reading and correcting the manuscript. M.E. thanks the Deutsche Forschungsgemeinschaft for a postdoctoral fellowship (Grant Er 214/1-1).

[1] U. Haeberlen, *High Resolution NMR in Solids—Selective Averaging* (Academic, New York, 1976).
[2] M. Mehring, *Principles of High Resolution NMR in Solids* (Springer, Berlin, 1983).
[3] K. Schmidt-Rohr and H. W. Spiess, *Multidimensional Solid State NMR and Polymers* (Academic, London, 1994).
[4] P. Tekely, P. Palmas, and D. Canet, J. Magn. Reson. A **107**, 129 (1994).
[5] I. J. Shannon, K. D. M. Harris, and S. Arumugam, Chem. Phys. Lett. **196**, 588 (1992).
[6] J. R. Sachleben, S. Caldarelli, and L. Emsley, J. Chem. Phys. **104**, 2518 (1996).
[7] A. E. Bennett, C. M. Rienstra, M. Auger, K. V. Lakshmi, and R. G. Griffin, J. Chem. Phys. **103**, 6951 (1995).
[8] E. R. Andrew, A. Bradbury, and R. G. Eades, Nature (London) **182**, 1659 (1958).
[9] E. R. Andrew, A. Bradbury, and R. G. Eades, Nature (London) **183**, 1802 (1959).
[10] I. J. Lowe, Phys. Rev. Lett. **2**, 285 (1959).
[11] D. L. VanderHart, W. L. Earl, and A. Garroway, J. Magn. Reson. **44**, 361 (1981).
[12] K. T. Mueller, B. Q. Sun, G. C. Chingas, J. W. Zwanziger, T. Terao, and A. Pines, J. Magn. Reson. **86**, 470 (1990).
[13] A. Llor and J. Virlet, Chem. Phys. Lett. **152**, 248 (1988).
[14] A. Samoson, E. Lippmaa, and A. Pines, Mol. Phys. **65**, 1013 (1988).
[15] H. J. Reich, M. Jautelat, M. T. Messe, F. J. Weigert, and J. D. Roberts, J. Am. Chem. Soc. **91**, 7445 (1969).
[16] B. Birdsall, N. J. M. Birdsall, and J. Feeney, J. Chem. Soc. Chem. Commun. **1972**, 316.
[17] A. Abragam, *Principles of Nuclear Magnetism* (Clarendon, Oxford, 1961).
[18] D. Freude and J. Haase, NMR Basic Principles and Progress **29**, 1 (1993).
[19] D. L. VanderHart, J. Chem. Phys. **84**, 1196 (1986).
[20] M. P. Augustine, K. W. Zilm, and D. B. Zax, J. Chem. Phys. **98**, 9432 (1993).
[21] M. Ernst, A. C. Kolbert, K. Schmidt-Rohr, and A. Pines, J. Chem. Phys. **104**, 8258 (1996).
[22] D. P. Raleigh, A. C. Kolbert, T. G. Oas, M. H. Levitt, and R. G. Griffin, J. Chem. Soc. Faraday Trans. 1 **84**, 3691 (1988).
[23] T. G. Oas, R. G. Griffin, and M. H. Levitt, J. Chem. Phys. **89**, 692 (1988).
[24] M. H. Levitt, T. G. Oas, and R. G. Griffin, Isr. J. Chem. **28**, 271 (1988).
[25] A. C. Kolbert, D. P. Raleigh, R. G. Griffin, and M. H. Levitt, J. Magn. Reson. **89**, 133 (1990).
[26] R. R. Ernst, G. Bodenhausen, and A. Wokaun, *Principles of Nuclear Magnetic Resonance in One and Two Dimensions* (Clarendon, Oxford, 1987).
[27] D. M. Brink and G. R. Satchler, *Angular Momentum* (Clarendon, Oxford, 1993).
[28] M. E. Rose, *Elementary Theory of Angular Momentum* (Dover, New York, 1995).
[29] U. Haeberlen and J. S. Waugh, Phys. Rev. **175**, 453 (1968).
[30] M. Goldman, P. J. Grandinetti, A. Lor, Z. Olejniczak, J. R. Sachleben, and J. W. Zwanziger, J. Chem. Phys. **97**, 8947 (1992).
[31] U. Haeberlen and J. S. Waugh, Phys. Rev. **175**, 453 (1968).
[32] W. P. Aue, D. J. Ruben, and R. G. Griffin, J. Chem. Phys. **80**, 1729 (1984).
[33] D. Suter, A. Pines, J. H. Lee, and G. Drobny, Chem. Phys. Lett. **144**, 324 (1988).
[34] A. Abragam and J. Winter, Comput. Rend. **249**, 1633 (1959).
[35] M. Mehring, G. Sinning, and A. Pines, Z. Phys. B **24**, 73 (1976).
[36] G. Sinning, M. Mehring, and A. Pines, Chem. Phys. Lett. **43**, 382 (1976).
[37] M. Mehring and G. Sinning, Phys. Rev. **15**, 2519 (1977).
[38] M. M. Maricq, J. Chem. Phys. **86**, 5647 (1987).
[39] M. M. Maricq, Adv. Magn. Reson. **14**, 151 (1990).
[40] M. A. Eastman, P. J. Grandinetti, Y. K. Lee, and A. Pines, J. Magn. Reson. **98**, 333 (1992).
[41] J. Lindgren and I. Olovsson, Acta Cryst. B **24**, 554 (1968).
[42] M. H. Wann, Ph.D. thesis, SUNY at Stony Brook, New York, 1993.
[43] S. R. Hartmann and E. L. Hahn, Phys. Rev. **128**, 2042 (1962).
[44] A. Pines, M. G. Gibby, and J. S. Waugh, J. Chem. Phys. **56**, 1776 (1972).
[45] J. Schaefer and E. O. Stejskal, J. Am. Chem. Soc. **98**, 1031 (1976).
[46] D. Michel and F. Engelke, NMR Basic Principles Prog. **32**, 69 (1994).
[47] P. J. Grandinetti, J. H. Baltisberger, A. Llor, Y. K. Lee, U. Werner, M. A. Eastman, and A. Pines, J. Magn. Reson. A **103**, 72 (1993).
[48] D. J. States, R. A. Haberkorn, and D. J. Ruben, J. Magn. Reson. **48**, 286 (1982).
[49] M. H. Levitt and R. Freeman, J. Magn. Reson. **43**, 502 (1981).
[50] M. H. Levitt and R. Freeman, and T. Frenkiel, J. Magn. Reson. **47**, 328 (1982).
[51] A. J. Shaka, J. Keeler, T. Frenkiel, and R. Freeman, J. Magn. Reson. **52**, 335 (1983).
[52] A. J. Shaka, J. Keeler, and R. Freeman, J. Magn. Reson. **53**, 313 (1983).
[53] S. A. Smith, T. O. Levante, B. H. Meier, and R. R. Ernst, J. Magn. Reson. A **106**, 75 (1994).
[54] V. B. Cheng, H. H. Suzukawa, and M. Wolfsberg, J. Chem. Phys. **59**, 3992 (1973).